# PAPER N

# DIFFRACTION TOMOGRAPHY IN A DISPERSIVE AND ATTENUATIVE MEDIUM

*Guan Y. Wang*

## ABSTRACT

In crosswell experiments, the conjugate symmetry of the object spectrum already exits, and it is not necessary to assume nonattenuative scattering. The conventional diffraction tomography is modified to include the evanescent mode in the backpropagation reconstruction to simultaneously invert wave fields for both the formation velocities and the attenuation coefficients. The method permits one not only to extract information about complex valued object function but also enables one to avoid discarding the data which would otherwise be through away by gathers in the situation of "over-sampling". In addition, by including attenuation, the inversion becomes more stable because of the symmetrical mathematical operations embodied in the diffraction tomography and the additional constraints from utilizing whole data set available. Forward modeling is carried out by incorporating Biot-Gassmann theory into a self consistent dispersion and attenuation model, and the velocity and attenuation are therefore, represented as the function of porosity, fluid content and the composition of the rock.

## INTRODUCTION

Diffraction tomography has its origins in geometric optics, is an inversion of the monofrequency wave field based on a linearization of the acoustic wave equation, and has notable similarities in its implementation to seismic migration. There are a number of seismic inversion and imaging techniques that derive from linearization of wave equation by Bron approximations. In this study we extend the technique of filtered backpropagation, as developed by Devaney (1982, 1984), Harris (1987), Wu and Toksoz (1987) to crosswell experiments in a dispersive and attenuative medium. For other configurations, such as vertical seismic profile (VSP) and surface reflection profile (SRP), the coverage is obtained by making use of the conjugate symmetry of the spectrum of a real valued function. The object function at any location is directly related to the local wave number, and is clearly real valued only for non-attenuating media. In crosswell experiments however, the conjugate symmetry of the object spectrum already exits, and it is not necessary to assume nonattenuative scattering. By including attenuation mode, the diffraction tomography in cross-well surveys can be used to extract information about complex valued object function, which providing a tool for simultaneously inverting wave fields for both formation velocities and the attenuation coefficients.

Assuming a linear visco-acoustic scattering model, i.e. including attenuation in the medium parameterization, a Fourier backpropagation reconstruction method is developed. The algorithm differs the conventional diffraction tomography in that the evanescent modes are not eliminated in the calculations. This is important not only because the attenuation coefficient can be recovered but also because the inversion becomes more stable as large data set, which severs as additional constraints, is used in the computation. The forward modeling is carried out by incorporated the Biot-Gassmann theory into a self consistent dispersion and attenuation model. The velocity and attenuation can, therefore, be represented as the function of porosity, fluid content and the composition of the rock. The results of the synthetic data inversion is excellent comparing to the model. The structural content in the reconstructed images of the field data is consistent with those of obtained with the techniques of cross well reflection imaging (Lazarators, et. al 1992) and crosswell migration (Mo, et. al, 1993). On the other hand, the values of the velocity and the attenuation coefficient can not be trust since the large contrast between the inhomogeneities and the background in the study area. A variable background method is needed and will be address in another paper.

## AN INVERSE SCATTERING MODEL OF A LOSSY MEDIUM

Consider an acoustic wave propagating in a linear visco medium. The corresponding wave equation can be written as

$$\nabla^2 P = b\frac{\partial P}{\partial t} + \frac{1}{c^2}\frac{\partial^2 P}{\partial t^2} \tag{1}$$

where b is the attenuation coefficient and c is the propagation velocity. In frequency domain, equation (1) becomes

$$\nabla^2 P(r,\omega) = (-i\omega b - \frac{\omega^2}{c^2}) P(r,\omega) \qquad (2)$$

let $P = P^0 + P^s$, and assume Born approximation, we set up the following linear inverse scattering model

$$P^s(s,g) = -\iint \{ik_{i0} o_i(r) + k_{r0} o_r(r)\} G(s,r) G(r,g) d^2 r \qquad (3)$$

where

$$o_i(r) = (1 - \frac{b(r)}{b_0}), \qquad o_r(r) = (1 - \frac{c_0^2}{c^2(r)})$$

are the real and imaginary part of the object function. In crosswell surveys the conjugate symmetry already exits, and it is not necessary to assume nonattenuative scattering. For a line source in the 2-D medium, the Green's function in equation (3) is the second kind and zero order Hankel function, i.e.

$$G(s,r) = H_0^{(2)}(\tilde{k}_0 |s-r|), \qquad G(r,g) = H_0^{(2)}(\tilde{k}_0 |r-g|)$$

where $\tilde{k}_0$ is the complex wave number. Obviously, G(s,r) represent a cylindrical wave with attenuation from the source to image location r and G(r,g) for a cylindrical wave from r to the receiver, as indicated in Figure 1.

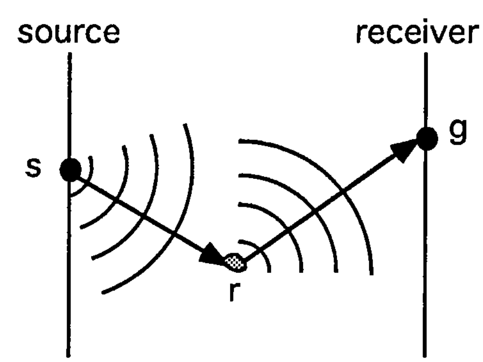


Fig. 1. The physical meaning of the G(s,r) and G(r,g)

The Fourier transforms of G(s,r) and G(r,g) along s and g are

$$F\{H_0^{(2)}(\tilde{k}_0|r-g|)\}(k_g)=\frac{2}{\gamma_g}e^{-i\gamma_g(x-x_g)-ik_gz}$$

and

$$F\{H_0^{(2)}(\tilde{k}_0|s-r|)\}(k_g)=\frac{2}{\gamma_s}e^{-i\gamma_s(x_s-x)-ik_sz}$$

Taking Fourier transform of equation (3) along source and receiver lines, which corresponding to plane wave decomposition, the spectrum of the scattering field is

$$P^s(x_g,x_s;k_g,k_s)=-\frac{e^{-i(\gamma_sx_s-\gamma_gx_g)}}{4\gamma_s\gamma_g}\iint\{k_{r0}^2o_r(r)+ik_{i0}o_i(r)\}e^{-i(\gamma_g-\gamma_s)x-i(k_g+k_s)z}dxdz \qquad (4)$$

where

$$\gamma_s^2=\tilde{k}_0^2-k_s^2 \qquad \gamma_g^2=\tilde{k}_0^2-k_g^2$$

are complex horizontal wave number. If we let

$$k_z=k_s+k_g \qquad s_x=i(\gamma_s-\gamma_g)$$

then equation (4) is a Laplace transform in x-direction and Fourier transform in z-direction. Therefore, the object function can be evaluated via the inverse Laplace and Fourier transforms, i.e.

$$\tilde{o}(r)=\frac{-1}{(2\pi)^2i}\iint P^s(x_g,x_s;k_g,k_s)4\gamma_s\gamma_ge^{i(\gamma_sx_s+\gamma_gx_g)}e^{s_xx+ik_zz}|J|dk_sdk_g \qquad (5)$$

where

$$\tilde{o}(r)=k_{r0}^2o_r(r)+ik_{i0}o_i(r)$$

Of course, this can be done only formally, because the numerical inverse Laplace transform is unstable. Other algorithms are needed. A possible scenario is to discreatize the equation (4) and use least square with constraints to form a linear system of equations. Since we are dealing with tomographic data set which is quite large usually, heavy computations are involved to solve the linear system. In the following we will develop a Fourier backpropagation reconstruction method.

## FOURIER DIFFRACTION RECONSTRUCTION FOR A LOSSY MEDIUM

In this section, we modify conventional diffraction tomography to include the evanescent mode in the backpropagation. This corresponds to allow wave numbers $k_s$, $k_g$ are larger or smaller than $k_0$ in the situation without attenuation. Denote $\tilde{k}_0 = \alpha + i\beta$ and let $\gamma_s = A_s + iB_s$, we have

$$A_s = \pm \frac{[\alpha^2 - \beta^2 - k_s^2]^{1/2}}{\sqrt{2}} \sqrt{\sqrt{1 + (\frac{2\alpha\beta}{\alpha^2 - \beta^2 - k_s^2})^2} + 1} \tag{6}$$

$$B_s = \pm \frac{[\alpha^2 - \beta^2 - k_s^2]^{1/2}}{\sqrt{2}} \sqrt{\sqrt{1 + (\frac{2\alpha\beta}{\alpha^2 - \beta^2 - k_s^2})^2} - 1} \tag{7}$$

Similarly let $\gamma_g = A_g + iB_g$ and $A_g$, $B_g$ are obviously in the same form as that of $A_s$ and $B_s$ except that the subscripts are different, i.e.

$$A_g = \pm \frac{[\alpha^2 - \beta^2 - k_g^2]^{1/2}}{\sqrt{2}} \sqrt{\sqrt{1 + (\frac{2\alpha\beta}{\alpha^2 - \beta^2 - k_g^2})^2} + 1} \tag{8}$$

$$B_g = \pm \frac{[\alpha^2 - \beta^2 - k_g^2]^{1/2}}{\sqrt{2}} \sqrt{\sqrt{1 + (\frac{2\alpha\beta}{\alpha^2 - \beta^2 - k_g^2})^2} - 1} \tag{9}$$

Substitute the horizontal wave number $\gamma_s$ and $\gamma_g$ into equation (4) we have

$$P^s(x_g, x_s; k_g, k_s) = -\frac{e^{-i(\gamma_s x_s + \gamma_g x_g)}}{4\gamma_s \gamma_g} \iint \tilde{o}(x,z) e^{-i(A_s + iB_s - A_g - iB_g)x - i(k_s + k_g)z} dxdz \tag{10}$$

Now consider the integral along variable x

$$\int_{-\infty}^{\infty} \tilde{o}(x)e^{-(B_g-B_s)x+i(A_g-A_s)x}dx$$

which is equivalent to

$$\int_c \tilde{o}(s)e^{[-(B_g-B_s)+i(A_g-A_s)]s}ds =$$
$$\int_c \tilde{o}(s)e^{[-(B_g-B_s)x-(A_g-A_s)y]+i[-(B_g-B_s)y+(A_g-A_s)x]}ds$$

in the s plane. Choosing a path such that $-(B_g-B_s)x-(A_g-A_s)y=0$ as indicated in Figure 2, we have

$$\int_c \tilde{o}(s)e^{[-(B_g-B_s)+i(A_g-A_s)]s}ds =$$
$$\frac{\sqrt{(B_g-B_s)^2+(A_g-A_s)^2}}{(B_g-B_s)}\int_c \tilde{o}(x)e^{i\frac{(A_g-A_s)^2+(B_g-B_s)^2}{(A_g-A_s)}x}dx \tag{11}$$

Since the attenuation of seismic wave is weak, the angle between the path s and axis x is very small. Consequently $\tilde{o}(s) \approx \tilde{o}(x)$ for finite x. For large x we assume $\tilde{o}(s)=\tilde{o}(x)=0$, as we only interested in finite borehole separation x.

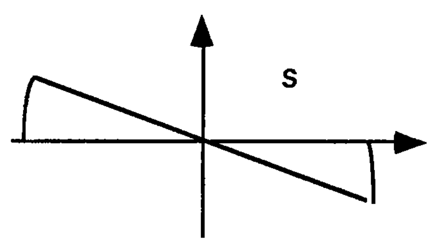


Fig. 2. The integral path in s-plane

Substitute equation (11) into equation (10) we have

$$P^s(x_g,x_s;k_g,k_s) = -\frac{e^{i(\gamma_s x_s-\gamma_g x_g)}}{4\gamma_s\gamma_g}\left|\frac{\sqrt{(B_g-B_s)^2+(A_g-A_s)^2}}{A_g-A_s}\right|\iint \tilde{o}(x,z)e^{-i(k_x x+k_z z)}dxdz \tag{12}$$

where

$$K_x = \frac{(A_g - A_s)^2 + (B_g - B_s)^2}{A_g - A_s} \qquad K_z = k_s + k_g$$

The object function can therefore, be evaluated via inverse Fourier transform, That is

$$\tilde{o}(x,z) = \frac{1}{(2\pi)^2} \int \frac{4\gamma_s \gamma_g (A_g - A_s)}{\sqrt{(B_g - B_s)^2 + (A_g - A_s)^2}} e^{i(\gamma_s x_s + \gamma_g x_g)} P^s(k_s, k_g) e^{i(K_x x + K_z z)} |J| dk_s dk_z \quad (13)$$

where J is Jacobean transformation matrix.

Equation (13) differs conventional diffraction tomography in that it includes the evanescent modes. This is important in two aspects: 1) the algorithm is more stable since evanescent mode acting as a constraint; 2) we do not have to throw away the data which usually are large gathers.

## THE SPECTRUM COVERAGE OF THE ATTENUATIVE SCATTERING

Most of physical process we interested can be described with following formal differential operator

$$L = \nabla^2 - \frac{1}{c^2}\frac{\partial^2}{\partial t^2} + g \quad (14)$$

In frequency domain, the relation of the wave number and frequency is

$$k(\omega) = \frac{\sqrt{\omega^2 + g}}{c} \quad (15)$$

or equivalently, the relation between the phase and group velocity is

$$c_g = c_\varphi \frac{\omega}{\sqrt{\omega^2 + g}} \quad (16)$$

These relations are so called dispersion equations and generally are nonlinear as indicated in Figure 3. From the differential operator (14) we can see that dispersion/attenuation can be caused by the nature of the medium, inhomogeneities and the geometrical dimension of the

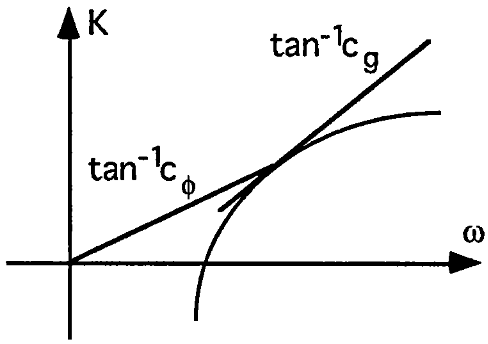


Fig. 3. Dispersion relation. $c_\varphi$ is the phase velocity and $c_g$ group velocity

problem. In the case of the scattering model we discussed

$$\nabla^2 P = b\frac{\partial P}{\partial t} + \frac{1}{c^2}\frac{\partial^2 P}{\partial t^2}$$

In frequency domain

$$-(k_x^2 + k_z^2)P(k_x, k_z, \omega) = (-i\omega b - \frac{\omega^2}{c^2})P(k_x, k_z, \omega)$$

and the dispersion equation is

$$k_x^2 + k_z^2 = (i\omega b + \frac{\omega^2}{c^2}) \tag{17}$$

In equation (17), the relation of the components of the wave vectors reflects the different modes of the propagation. For example, if b in equation (17) is zero, then

$$k_x = \sqrt{\frac{\omega^2}{c^2} - k_z^2} \qquad k_z = \pm n\frac{2\pi}{L}, \qquad n = 0,1,\ldots$$

where $k_z$ is set as an independent variable. For the certain cutoff of the vertical wave number $k_z = k_c \geq \frac{\omega^2}{c^2}$, the propagation in horizontal switch to evanescent mode because the horizontal wave number $k_x$ becomes pure imaginary, as shown in Figure 4.

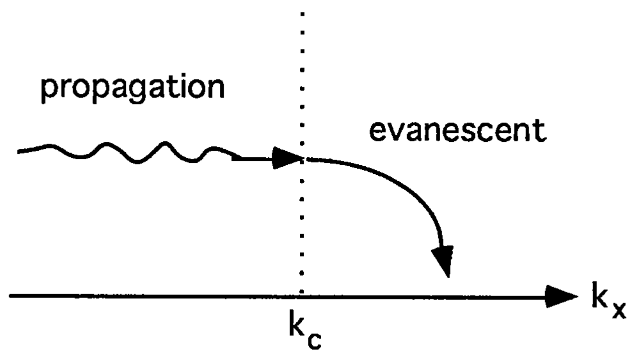


Fig. 4 The propagation and evanescent regions for lossless medium

In cross-well geometry, the horizontal and vertical wave vectors are $K_x = \gamma_s - \gamma_g$, and $K_z = k_s + k_g$ respectively, where $\gamma_s^2 = k_0^2 - k_s^2$, and $\gamma_g^2 = k_0^2 - k_g^2$. For $|k_g| \leq k_0$ or $|k_s| \leq k_0$, the spectrum coverage of the propagation wave is the shadow area shown in Figure 5a which is relatively small. However, for all possible values of $k_s$ and $k_g$, i.e. include evanescent modes, the spectrum coverage is the shadow area shown Fig. 5b which is larger than that of 5a.

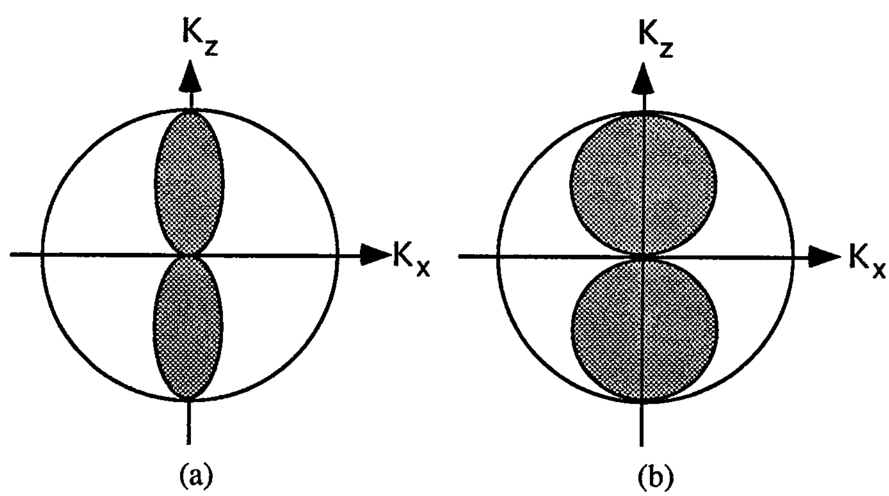


Fig. 5 The coverage of the scattering field spectrum: (a) only for propagation mode, (b) for both of propagation and evanescent modes

In conventional diffraction we assume nonattenuative scattering, i.e. when $|k_s|$ or $|k_g|$ is large than $k_0$, the data is discarded in the name of over sampling. We believe first the discarded data are important in terms of constraining the inversion and should be utilized; second in some case we have to consider attenuation and it is inevitable to deal with complex wave number. In a lossy medium

$$k_x = \sqrt{\frac{\omega^2}{c^2} + i\omega b - k_z^2} \tag{18}$$

The propagation and the evanescent modes always coexist, since the dispersion/attenuation is not solely the results of geometrical dimension of the wave propagation but also the property of the medium.

## A SELF CONSISTENT DISPERSION AND ATTENUATION MODEL

In this section, Biot-Gassmann theory is cooperated into a self consistent dispersion and attenuation model. Therefore the velocity and attenuation can be represented as the function of porosity, fluid content and the composition of the rock. Assuming the creep function satisfy a power law of the time, i.e.

$$\psi(t) = \begin{cases} (t/t_0)^{2\gamma} / M_0\Gamma(1+2\gamma) & t \geq 0 \\ 0 & t < 0 \end{cases} \tag{19}$$

and constant Q model. The velocity and 1/Q can be derived as (Kjartansson, 1979),

$$v = v_0(\frac{\omega}{\omega_0})^\gamma \cos\frac{\pi}{2}\gamma \qquad 1/Q = \tan(\pi\gamma) \tag{20}$$

where $\gamma$ is to be determined. The are a lot of debt about what value of the $\gamma$ could be.

In this study, we propose to incorporate the Gassmann and Boit's velocity limits into the above velocity dispersion equation. consequently, $\gamma$ can be determined in terms of wave property in porous media. Velocities at high and low frequency limits are

$$v_l = v_0(\frac{\omega_l}{\omega_0})^{\gamma}\cos\frac{\pi}{2}\gamma \qquad v_h = v_0(\frac{\omega_h}{\omega_0})^{\gamma}\cos\frac{\pi}{2}\gamma \tag{21}$$

Notice that the frequency range here is from zero to the frequency at which nonlinear effects occur. The velocity limits $v_l$ and $v_h$ is estimated from Boit-Gassmann theory (Biot, 1956a, Gassmann, 1951, Winkler, 1985)

$$\rho_c v_{pl}^2 = \frac{(k_s - k_b)^2}{k_s[1-\Phi-k_b/k_s+\Phi k_s/k_f]} + k_b + \frac{4}{3}N \tag{22}$$

$$\rho_c v_{sl}^2 = N \tag{23}$$

$$\rho_c v_{ph}^2 = \frac{A+[A^2-4B(PR-Q^2)]^{1/2}}{2B} \tag{24}$$

$$\rho_c v_{sh}^2 = \frac{N}{(1-\Phi)\rho_s + (1-1/\alpha)\Phi\rho_f} \tag{25}$$

where

$\Phi$ = porosity
$k_s$ = bulk modulus of the solid material
$k_f$ = bulk modulus of the fluid
$k_b$ = bulk modulus of the dry frame
$N$ = shear modulus of the dry frame
$\rho_c$ = bulk density of fluid-saturated rock
$\rho_s$ = density of the solid material
$\rho_f$ = density of the fluid

Substitute above limit velocities in to equation (21), the $\gamma_p$ and $\gamma_s$ is solved. Therefore the complex velocity (20) is represent as the function of porosity, fluid content and the composition of the rock. With the input displayed in Table 1, and the velocities at frequency 1000 Hz are calculated as shown in Table 2.

Table 1.

| thickness | $\Phi$ | $\rho_0$ | $k_0$ | $v_p$ (dry) | $v_s$ (dry) | $\rho_f$ | $k_f$ |
|---|---|---|---|---|---|---|---|
| ~ | 0.084 | 2650 | 38 | 5480 | 2990 | 1000 | 2.51 |
| 60 | 0.10 | 2650 | 38 | 4510 | 2770 | 1000 | 2.51 |
| ~ | 0.084 | 2650 | 38 | 5480 | 2990 | 1000 | 2.51 |

Table 2. Frequency = 1000 Hz

| thickness | $v_p$ | $v_s$ | $Q_p$ | $Q_s$ |
|---|---|---|---|---|
| ~ | 5447 | 2949 | 566.33 | 81.63 |
| 60 | 4563 | 2732 | 2170.98 | 782.75 |
| ~ | 5447 | 2957 | 566.33 | 851.63 |

With the obtained velocities and Q's above, we can calculate the acoustic fields in the composite medium according to linear visco-acoustic equation (1) or (2). The forward modeling is calculated with program VESPA and directly output in frequency domain.

## NUMERICAL EXAMPLES

In this section, we test the reconstruction algorithm developed above with the examples both of synthetic and field data. The first example consists of a 1-D three layer model. The corresponding total field and reference field in frequency domain is shown in figure 6, where the fields are averaged in the frequency range of 950 to 1050 Hz. It is interesting to notice that the inhomgeneity shows up in frequency domain more clear than in time domain.

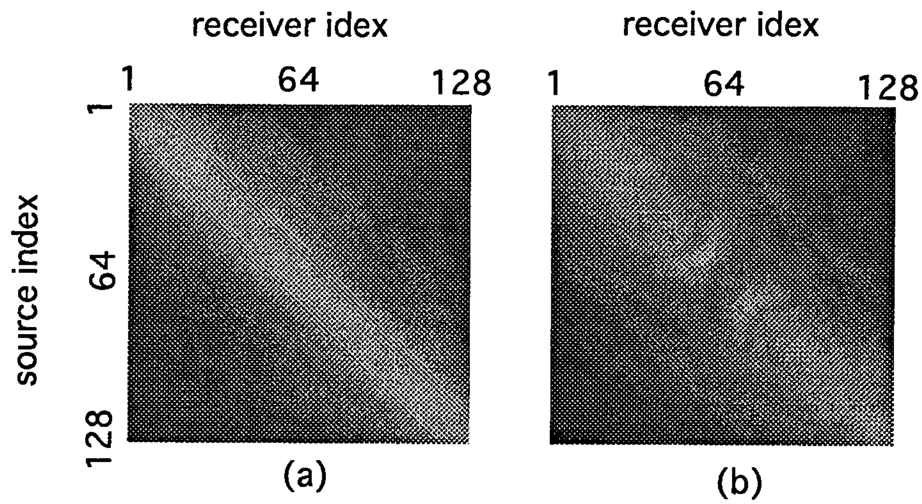


Fig. 6. Total field and background in frequency domain
(a) total field and (b) incident field

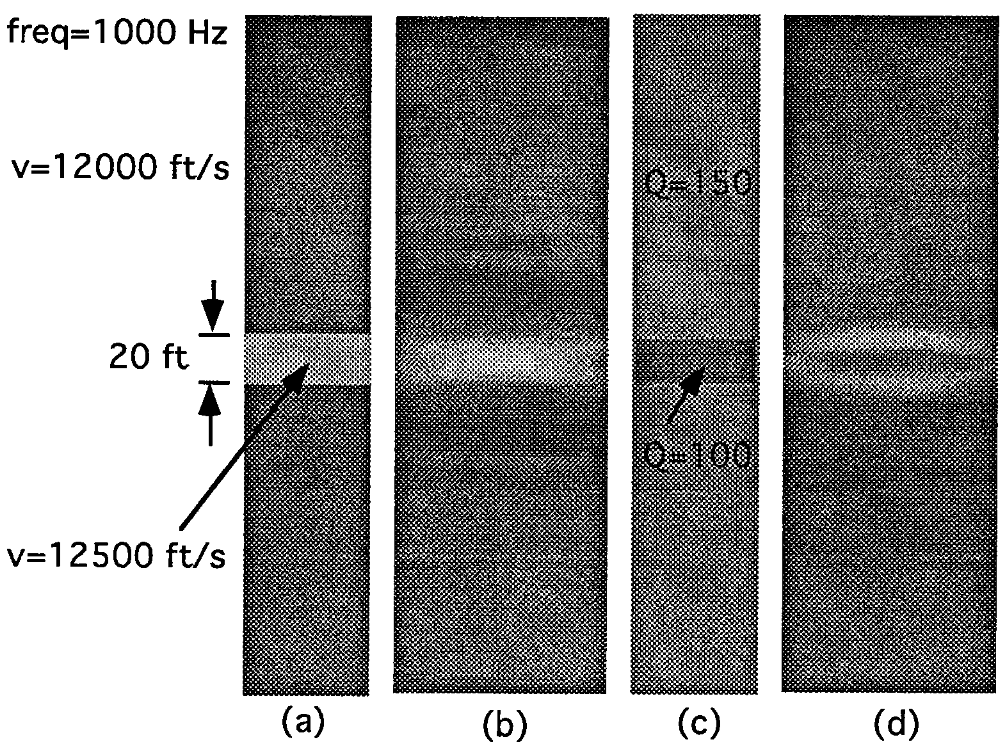


Fig. 7 Reconstruction with synthetic data. (a) 1-D velocity model
(b)reconstruction of the velocity, and (c) 1-d Q model and
(d) reconstruction of the attenuation coefficient.

The inversion results are indicated in Figure 7. We can see from Figure 7b that while velocity are reconstructed almost perfect regarding to the discontinuities, the image of the attenuation coefficient in Figure 7d is smear out at the boundaries comparing with Figure 7c

The second example is the inversion with the field data from a West Texas test site. We are aware that in the area being studied the velocity contrast is strong and the Born

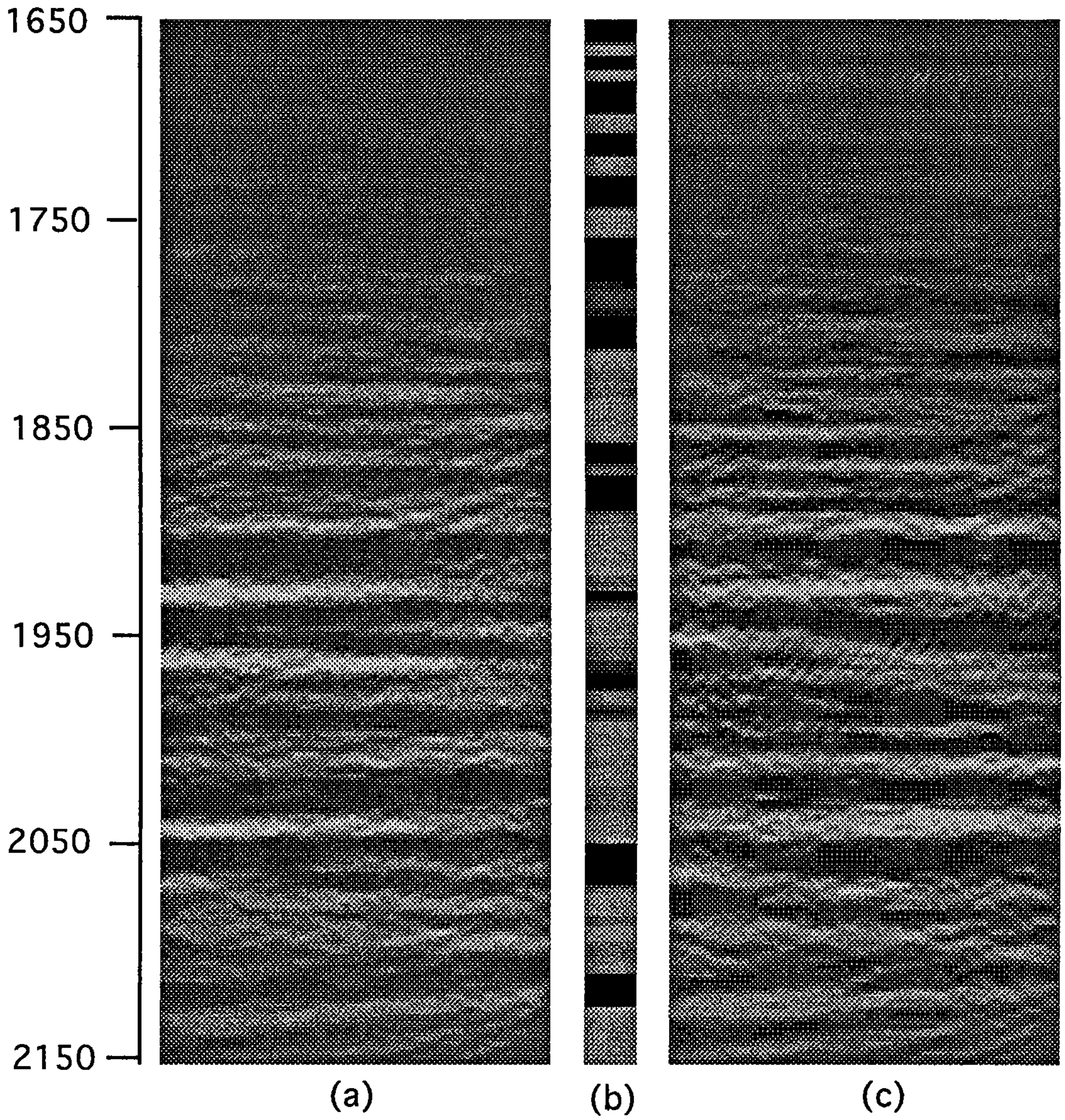


Fig. 8 Inversion of the field data from West Texas. (a) the reconstruction of the velocity, (b) the well log in suit, and (c) the reconstruction of the attenuation coefficient.

approximation of a constant background is not valid. This issue will be addressed in other related studies. Here, as a tentative test, a homogeneous background is applied in the Figure 8. As we can see the structural content in the reconstructed images is comparable to those of obtained with the techniques of cross well reflection imaging (Lazaratos, et. al, 1992) and the crosswell migration (Mo, 1993). On the other hand, the values of the velocity and the attenuation coefficient can not be trust since the large contrast between the inhomogeneities and the background, since the weak inhomogeneity inverse model is valiant at first place.

## CONCLUSIONS

By incorporating Biot-Gassmann theory into a self consistent dispersion and attenuation model, and the velocity and attenuation can be represented as the function of porosity, fluid content and the composition of the rock. By including evanescent mode in the inversion, the algorithm not only permit diffraction tomography in cross-well surveys to be used to extract information about complex valued object function and simultaneously invert wave fields for both formation velocities and the attenuation coefficients, but also enable one to avoid discarding the data which would otherwise be through away by large number of gathers in the situation of "over-sampling". In addition, by including attenuation, the inversion becomes more stable because of the symmetrical mathematical operations embodied in the diffraction tomography and the additional constraints from utilizing whole data set available. The inversion results from the synthetic and field data indicate that the algorithm is robust and efficient. The structural content in the reconstructed images of the field is comparable to those of obtained with the techniques of cross well reflection imaging and crosswell migration.

## ACKNOWLEDGMENTS

I want to thank Mark Van Schaack for many useful comments and his help of using field data.

## REFERENCE

Biot, M. A. 1956a, Theory of propagation of elastic waves in a saturated porous solid. I. low-frequency range: J. Acoust. Soc. Am., 28, 168-178.

-- 1956b, Theory of propagation of elastic waves in a saturated porous solid. II High-frequency range: J. Acoust. Soc. Am. 28. 179-191

Devaney A. J., G. C. Sherman, 1982, Non-uniqueness in inverse source and scattering problems: IEEE Trans. Ant. propagat. AP-30, 1034.

Devaney, A. J., 1984, Geophysical diffraction tomography, IEEE Trans. Geosci. remote

Kjartansson E. 1979, Attenuation of seismic waves in rocks and applications in energy exploration, Ph.D thesis, Stanford University.

Gary Mavko and Diane Jizba, 1991: Estimating grain-scale fluid effects on velocity dispersion in rocks, Geophysics, **56**, 12.

Harris J. M., 1987, Diffraction tomography with arrays of discrete sources and receivers: IEEE trans. Geosci. and Remote Sensing, 25(4), 448-455.

Harris J. M., Ramm A. G., 1988, Inversion of the acoustic well to well data: Appl. Math. Lett. 1 (2), 127-131

Kenneth W. W, 1985, Estimates of velocity dispersion between seismic and ultrasonic frequency: Geophysics, **51**, 1.

Lazaratos, S. K. , Harris, J. M., Rector III, J. W. and Van Schaack M., High resolution cross well imaging of a west Texas carbonate reservoir: part 4. reflection imaging: SEG Expanded abstract

Mo, L., 1993, Cross-well migration of seismic data, Part II, field data, STP volume IV

Wu, R. and Toksoz, M. N. 1987, Diffraction tomography and multi-source holography applied to seismic imaging: Geophysics, **52**, 11-25.